A Broadband Microwave Fourier Transform Spectrometer, Especially Designed for Stark Effect Investigations of Almost Nonpolar Molecules; the Electric Dipole Moment and the Anisotropy in the Static Electric Polarizability Tensor of 1,1-Dideuteroallene, $D_2C=C=CH_2$

V. Meyer and D. H. Sutter

Abteilung Chemische Physik im Institut für Physikalische Chemie der Christian-Albrechts-Universität zu Kiel, Kiel, FRG

Z. Naturforsch. **48a**, 725–732 (1993); received March 26, 1993

A bridge type microwave Fourier transform spectrometer, equipped with flat oversized Stark cells and an operational range from 8 GHz to 40 GHz is described. As application we report the experimental determination of the vibronic ground state dipole moment and of the anisotropy in the static polarizability of 1,1-dideuteroallene. Our experimental values are: $\mu_a = 0.0053(2)$ D for the dipole moment, and $(\alpha_{\parallel} - \alpha_{\perp}) = 4.26(6) \cdot 10^{-24}$ cm^3, for the polarizability anisotropy.

1. Introduction

In view of its inherent high sensitivity and resolution, waveguide microwave Fourier transform spectroscopy (MWFT), first introduced by Flygare and coworkers in the early seventieth [1], is an ideal technique to study the Stark effect in the rotational spectra of near nonpolar molecules [2, 3]. The analysis of the splittings of the rotational transitions in an exterior electric field directly leads to the vibronic ground state expectation values for the electric dipole moment and for the anisotropies in the electric polarizability tensor, i.e. to molecular parameters which are of high interest in calculations of intermolecular forces at close range. In the following we describe a new bridge type MWFT spectrometer especially designed for such Stark effect studies. As a first application we present results obtained for 1,1-dideutero allene, $D_2C=C=CH_2$, whose small vibronic ground state dipole moment arises from the slight imbalance in the vibronic ground state structures at the $=CD_2$ and $=CH_2$ end. Our results differ considerably from data reported in an early pioneering microwave study [4], in which only weak and unresolved spectroscopic features could be analysed.

Reprint requests to Prof. Dr. D. H. Sutter, Abteilung Chemische Physik im Institut für Physikalische Chemie, Universität zu Kiel, Olshausenstraße 40–60, W-2300 Kiel 1, FRG.

2. Experimental

A block diagram of our spectrometer is shown in Fig. 1 (V-band version, i.e. microwave components specified for the 26.4 to 40 GHz range). As main difference with respect to a standard waveguide MWFT spectrometer, the in-band waveguide "absorption" cell is replaced by a pair of identical oversized cells, arranged in a bridge setup. One cell (the lower one in Fig. 1) contains the sample under investigation (pressure typically in the 1 to 10 mTorr range), the other cell is evacuated. In a bridge setup one can cope with the problems associated with the use of oversized cells, i.e. mode conversion to higher modes, which lead to comparatively long lasting resonances in the cell superimposed to the faint molecular transient emissions, and nevertheless one can still take advantage of their lower insertion loss, their reduced rate of wall collisions, and of the high homogeneity of the Stark-field which can be achieved in flat, oversized cells (see below). Our cells have an overall length of 3 m and an inner cross section of 10 mm by 47 mm. Each is equipped with a central Stark septum, 3 mm thick, which is running parallel to the broad face of the waveguide. These "Stark-plates" are supported and insulated from the waveguide walls by grooved teflon strips. To minimize reflections, the septa are symmetrically tapered at each end. Typical data characterizing their microwave transmission properties as tested with an hp 8757 C scalar network analyzer are a

0932-0784 / 93 / 0500-0725 $ 01.30/0. – Please order a reprint rather than making your own copy.

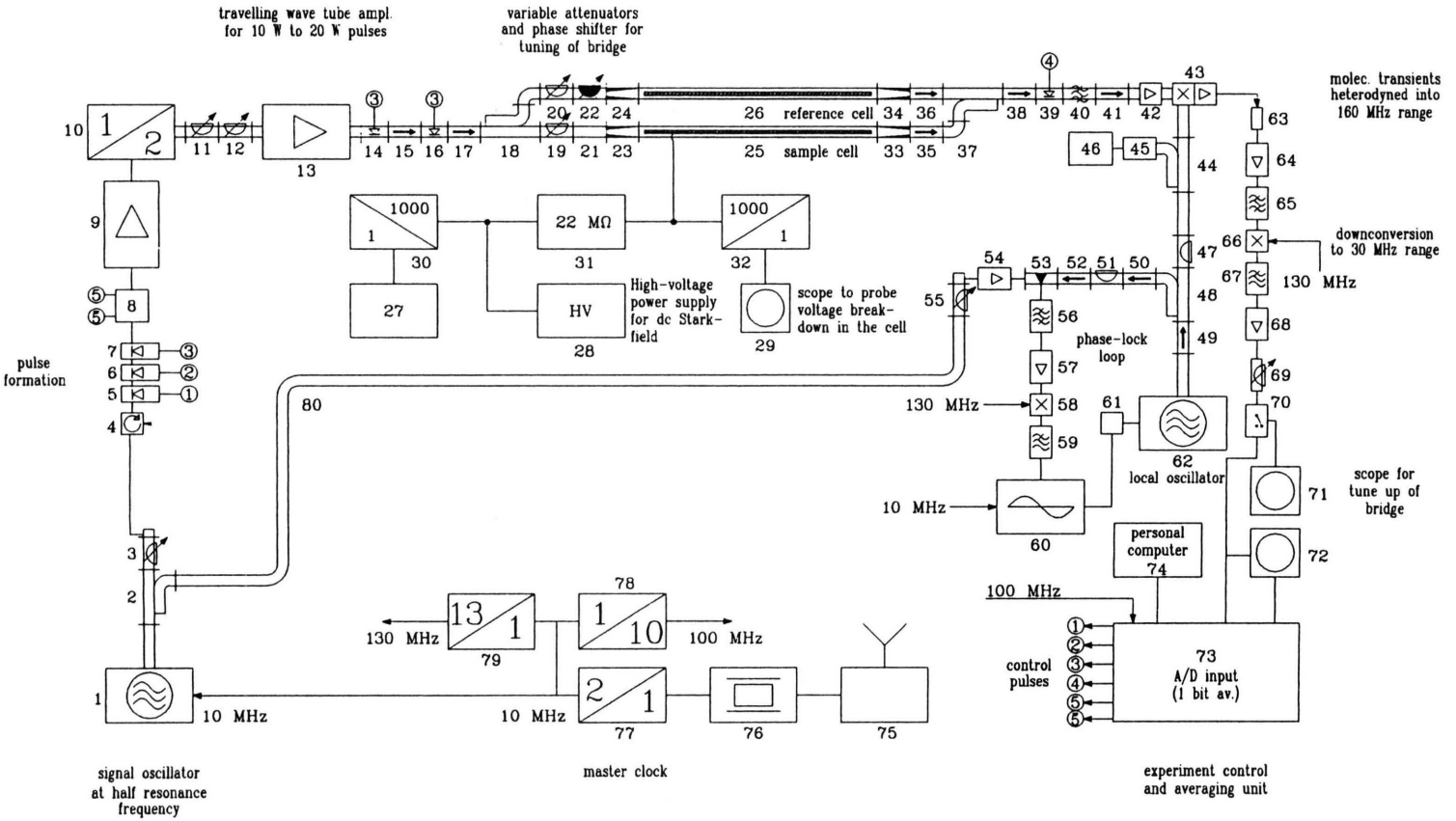

Fig. 1. Block diagram of the MWFT bridge spectrometer for Stark-effect investigations. Prior to each experiment the bridge is tuned such that the microwave pulses travelling through the system from left to right interfere destructively after recombination in the directional coupler at the end of the bridge set up (part 37). Problems, which in a single cell setup would be associated with unavoidable reflections at the end of the oversized sample cell, can thus be largely eliminated. Only the molecular emission signal which originates from the lower sample cell (the upper reference cell is evacuated) reaches the detector. If necessary, the sample cells can be cooled down to $-70\,^{\circ}C$ by methanol flowing through a cooling jacket. Both cells are mounted inside evacuated tubes in order to avoid deformations which otherwise might be caused by the external atmospheric pressure. For technical details compare also [5]. A list with the technical specifications of all components used in the present investigation may be ordered from the authors.

voltage standing wave ratio of 1.5 and an insertion loss of 3.5 dB at a microwave frequency of 24 GHz. When shifting from the X-band through the Ku-band and K-band to the V-band, only the microwave components have to be changed while the double cell and the intermediate frequency section of the spectrometer remain in place. In the following we briefly sketch how the V-band setup, explicitely shown in Fig. 1, operates. For technical details compare also [5].

In an experiment near resonance, short (1–3 μs) and intense (10–20 W) microwave pulses are used to drive the molecules coherently into mixed states (non-eigenstates). After the end of the pulse this results in a macroscopic polarisation of the gas sample which oscillates at the resonance frequency corresponding to the energy difference between the upper and lower level involved in the transition, and which leads to a transient molecular emission signal. Within 10 to 50 μs this signal decays. The decaytime is mainly determined by the loss of coherence as caused by collisions, Doppler dephasing, and, in a Stark-effect experiment, the inhomogeneity of the applied Stark field in the outer regions of the waveguide. This inhomogeneity leads to slightly different spacings of the energy levels of molecules experiencing different Stark fields and causes their wave trains to "get out of step" already shortly after the end of the exciting pulse. Behind the sample cell the faint molecular emission signal is amplified (in part 42 of Fig. 1) and downconverted into the 160 MHz range (in part 43) by heterodyning it against the strong local oscillator signal. After a second downconversion into the 30 MHz range (in part 66) the transient emission is sampled by a 1 bit A/D-converter at 10 ns intervals, and the data are stored in the memory of the home made experiment control and averaging unit (part 73, [6]). For near nonpolar molecules, such as $D_2C=C=CH_2$ studied here, the extremely faint transient emission from typically $5 \cdot 10^7$ to 10^8 excitations are recorded for a period of about 10 μs each and averaged up for noise compensation prior to the subsequent analysis.

As indicated above, the most serious problem associated with the use of oversized sample cells in a MWFT spectrometer is that mode conversion from the fundamental into higher modes (and vice versa) cannot be completely eliminated. These higher modes are unable to propagate in the adjacent in-band waveguides and thus bounce back and forth in the oversized cell. By reconversion to the fundamental mode, this leads to comparatively long lasting "pulse echoes". (Note that the power in the pulse falls into the 10 W range, while the molecular emission signal is in the 10^{-13} W range or even below.) As worked out in the Appendix of [7] such "pulse echoes" may degrade the sensitivity of the 1-bit averaging system to a degree which prevents the detection of the molecular emission. In a bridge-type setup, however, it is possible to overcome this problem in an elegant way. By proper adjustment of the phase shifter (part 22) and the attenuators (part 19 and 20) it is possible to fine-tune the bridge such that the pulse signals propagating through the two oversized cells interfere destructively after recombination in the directional coupler behind the cells (part 37). (In a tuned bridge the complete pulse power is dissipated in the absorber inside the directional coupler.) The same destructive interference also occurs for the pulse echoes. Sure enough, perfect tuning cannot be achieved, but in practice it is always possible to reduce the amplitude of the echoe well below the noise level, which is sufficient to preserve the full sensitivity of the system [7]. In contrast to the pulse echoes, the molecular transient emission originates only from one cell and thus does not suffer from destructive interference.

For 1,1-dideuteroallene, kindly provided by Beat Vogelsanger, Zürich [8], we studied the Stark-effect of the $J''_{K''_a K''_c} \rightarrow J'_{K'_a K'_c} = 1_{01} \rightarrow 0_{00}$ rotational transition near 15.7 GHz and all three $J'' \rightarrow J' = 2 \rightarrow 1$ transitions near 31.6 GHz. Stark-fields up to 14 kV/cm were applied. The spectrometer was calibrated using OCS as standard [9]. With the vectors of the Stark-field and the electric field of the incident microwave radiation parallel, the $\Delta M = 0$ electric dipole selection rule applied. Thus one Stark-satellite ($M = 0$) was observed for the $1 \rightarrow 0$ transition and two Stark-satellites ($M = 0$ and $M = \pm 1$) were observed for the $2 \rightarrow 1$ transitions. In order to give an idea of the quality of the spectra obtained with the spectrometer, we present two experimental results in Figure 2. The figure shows the MWFT power spectra calculated from the transient emission signals of the $2_{02} \rightarrow 1_{01}$ rotational transition in zero field and in a Stark-field fo 12.697 kV/cm. We note, however, that the final derivation of the line frequencies from the transient emission signals was not carried out by use of the Fourier transform technique, since this procedure may lead to distorted frequencies if closely spaced lines are investigated. (With reference to MWFT, this problem has been worked out in detail in the Appendix of [10].) Instead, the frequencies, amplitudes, decay times, and phases of

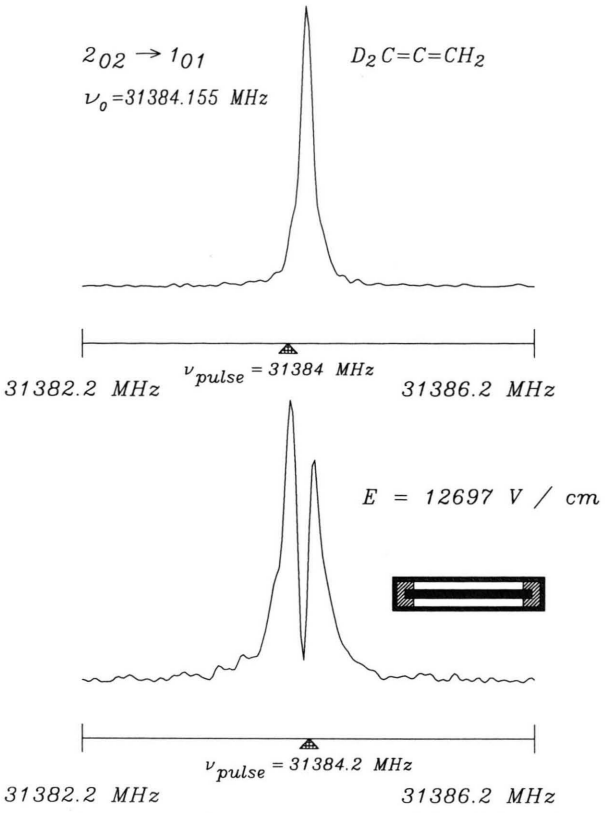

Fig. 2. Fourier transform power spectra deduced from the transient emissions from the $2_{02} \rightarrow 1_{01}$ rotational transition of $D_2C=C=CH_2$ in zero field (upper trace) and in a field of 12.697 kV/cm (lower trace). The insert shows the cross section of the sample cell. The Stark-voltage is applied to the central plate. The walls are grounded. With the electrical vectors of the incident microwave parallel to the Stark-field the electric dipole selection rule $\Delta M=0$ applies and the doublet represents the $M=0$ and $|M|=1$ Stark satellites. Sample pressure: 12 mTorr; temperature: 291 K; 10^3 data points sampled at 10 ns intervals; $65 \cdot 10^6$ averaging cycles. Prior to the Fourier analysis the 10^3 data points were complemented by $3 \cdot 10^3$ zeroes.

the satellite signals were directly fitted to the observed transient emissions by an iterative least squares procedure developed by Haeckel and Mäder [11]. Our results are listed in Table 1. Also listed in Table 1 is a Stark-shift of the $M=0$ satellite in the $1 \rightarrow 0$ transition observed earlier at Zürich by B. Vogelsanger. It fits nicely into our data. In the following section we comment on our analysis of the observed Stark-splittings.

3. Analysis of the Stark-Effect Splittings

For the analysis of the low-J Stark-effect splittings observed here we have used the rigid rotor Hamiltonian, supplemented by the potential energy of the vibronic ground state electric dipole moment, $\langle \boldsymbol{\mu} \rangle$, and of the field induced electric dipole moment, $\bar{\alpha} \cdot \boldsymbol{E}$, in the static exterior electric field, $\boldsymbol{E}$. Deuterium quadrupole coupling and the spin-rotation interaction of the hydrogen and the deuterium nuclei were neglected. Thus the Hamiltonian used here was of the form

$$\hat{H} = \hat{H}_{\text{rot}} + \hat{H}_{\text{Stark}} \tag{1}$$

with

$$H_{\text{Stark}} = -\boldsymbol{\mu} \cdot \boldsymbol{E} - \tfrac{1}{2} \boldsymbol{E} \cdot \bar{\alpha} \cdot \boldsymbol{E} . \tag{2}$$

In (1) $\bar{\alpha}$ is the (static) electric molecular polarizability tensor.

If referred to the molecular principal inertia axes system, the two contributions to our effective Hamiltonian may be written more explicitly as

$$\hat{H}_{\text{rot}} = h(A \hat{J}_a^2 + B \hat{J}_b^2 + C \hat{J}_c^2) . \tag{3}$$

and

$$\hat{H}_{\text{Stark}} = -\mu_a E_Z \cos(aZ) - \tfrac{1}{2} E_z^2 (\alpha_{aa} \cos^2(aZ) + \alpha_{bb} \cos^2(bZ) + \alpha_{cc} \cos^2(cZ)) . \tag{4}$$

In (3) A, B, and C are the rotational constants, h is Planck's constant, and $\hat{J}_g^2$ ($g=a, b, c$) are the squares of the components of the angular momentum operators in direction of the principal inertia axes. In (4) $\cos(gZ)$ ($g = a, b, c$) is used for the direction cosines between the gyrating principal inertia axes and the exterior field axis. The latter is assumed to point into the Z-direction of the laboratory frame.

In $D_2C=C=CH_2$ the a-axis, i.e. the axis corresponding to the smallest moment of inertia, points into the direction of the heavy atom chain, and the b-axis is parallel to the connection between the two deuterium nuclei. In (4) use has been made of the symmetry (D_{2d}). The only nonzero component of the electric dipole moment vector must point in direction of the heavy atom chain, and due to the mirror planes there are no nonzero off-diagonal elements in the polarizability tensor. Furthermore, it will be a good approximation to set $\alpha_{bb} = \alpha_{cc} = \alpha_\perp$, i.e. to neglect the slight deviation from the original cylindrical symmetry of the polarizability tensor which was introduced by asymmetric deuteration.

Since the rotational energies are by about four orders of magnitude larger than the Stark-effect contributions, we have treated $\hat{H}_{\text{Stark}}$ as a perturbation to the rigid rotor Hamiltonian, $\hat{H}_{\text{rot}}$. Within the eigenfunction basis of the rigid rotor the permanent dipole moment contributes only within second order pertur-

Table 1. Experimental and calculated Stark-effect splittings of the $1 \rightarrow 0$ and the three $2 \rightarrow 1$ rotational transitions of $D_2C=C=CH_2$ as observed by MWFT-spectroscopy. To demonstrate that the polarizability anisotropy and the electric dipole moment can be determined independently, we present their individual contributions to the Stark-splittings as calculated by (6) and (9).

E/V cm^{-1}	$\Delta\nu_{obs}$/ kHz	$\Delta\nu(\mu)_{calc}$/ kHz	$\Delta\nu(\alpha)_{calc}$/ kHz	$\Delta\nu_{obs}-\Delta\nu_{calc}$/ kHz
$J''_{K''_aK''_c} \rightarrow J'_{K'_aK'_c} = 1_{01} \rightarrow 0_{00}$, $\nu_{zerofield} = 15\,692.305$ MHz, $M=0$				
4 618	−17	5	−20	−2
5 772	−19	8	−32	5
6 927	−23	12	−46	11
8 200	−47 [a]	16	−64	1
$J''_{K''_aK''_c} \rightarrow J'_{K'_aK'_c} = 2_{02} \rightarrow 1_{01}$, $\nu_{zerofield} = 31\,384.155$ MHz, $M=0$				
6 923	11	−3	13	1
12 697	30	−11	44	−3
13 979	46	−14	53	7
$J''_{K''_aK''_c} \rightarrow J'_{K'_aK'_c} = 2_{02} \rightarrow 1_{01}$, $\nu_{zerofield} = 31\,384.155$ MHz, $\lvert M\rvert = 1$				
6 923	−35	3	−39	1
12 697	−119	9	−132	4
13 979	−141	11	−160	8
$J''_{K''_aK''_c} \rightarrow J'_{K'_aK'_c} = 2_{11} \rightarrow 1_{10}$, $\nu_{zerofield} = 31\,602.010$ MHz, $M=0$				
4 616	−17	1	−17	−1
5 770	−25	2	−27	0
6 924	−35	3	−39	1
8 113	−47	4	−54	3
9 253	−71	5	−70	−6
10 423	−81	6	−89	2
11 592	−103	8	−110	−1
12 724	−122	9	−132	1
13 989	−161	11	−160	−12
$J''_{K''_aK''_c} \rightarrow J'_{K'_aK'_c} = 2_{11} \rightarrow 1_{10}$, $\nu_{zerofield} = 31\,602.010$ MHz, $\lvert M\rvert = 1$				
4 616	−173	−168	1	−6
5 770	−263	−262	2	−3
6 924	−383	−377	3	−9
8 141	−518	−521	5	−2
9 461	−695	−704	6	3
10 429	−856	−856	7	−7
11 571	−1056	−1054	9	−11
12 734	−1255	−1276	11	10
13 961	−1510	−1534	13	11
$J''_{K''_aK''_c} \rightarrow J'_{K'_aK'_c} = 2_{12} \rightarrow 1_{11}$, $\nu_{zerofield} = 31\,166.058$ MHz, $M=0$				
4 616	−15	1	−17	1
5 770	−22	2	−27	3
6 924	−28	3	−39	9
8 081	−39	4	−53	10
9 243	−58	5	−70	7
10 413	−79	6	−89	4
11 560	−104	8	−110	−2
12 741	−134	9	−133	−10
13 970	−153	11	−160	−4
$J''_{K''_aK''_c} \rightarrow J'_{K'_aK'_c} = 2_{12} \rightarrow 1_{11}$, $\nu_{zerofield} = 31\,166.058$ MHz, $\lvert M\rvert = 1$				
4 616	170	169	1	0
5 770	272	265	2	5
6 924	379	381	3	−5
8 095	520	521	4	−5
9 246	686	679	6	1
10 339	879	859	7	13
11 557	1082	1061	9	12
12 717	1296	1285	11	0
14 005	1565	1559	13	−7

bation theory [12], while the polarizability already leads to first order contributions. We first treat the latter.

Since the polarizability contribution has exactly the same mathematical form as the magnetic susceptibility contribution in rotational Zeeman-effect spectroscopy [13], we can use the matrix elements derived earlier for the susceptibility contribution without having to go through the mathematical derivation again. We simply have to replace the magnetic field strength, H_Z, by the electric field strength, E_Z, and the magnetic susceptibility tensor elements, χ_{gg}, by the elements of the electric polarizability tensor, α_{gg}. The explicit expression to use for the calculation of the polarizability contribution to the energy levels thus takes the form

$$W_{\alpha(J,K_aK_c,M)} = -\tfrac{1}{2}\alpha E_Z^2 - E_Z^2 \frac{3M^2 - J(J+1)}{(2J-1)(2J+3)J(J+1)} \sum_{g=a,b,c} (\alpha_{gg} - \alpha)\langle \hat{J}_g^2 \rangle \quad (5)$$

(compare (III,12) of [13]). In (4) $\alpha = (\alpha_{aa} + \alpha_{bb} + \alpha_{cc})/3$ is the so-called (static) molecular bulk polarizability and $\langle \hat{J}_g^2 \rangle$ ($g = a, b, c$) are the asymmetric top expectation values for the squares of the components of the angular momentum corresponding to the overall rotation. For the low-J states of interest here, the

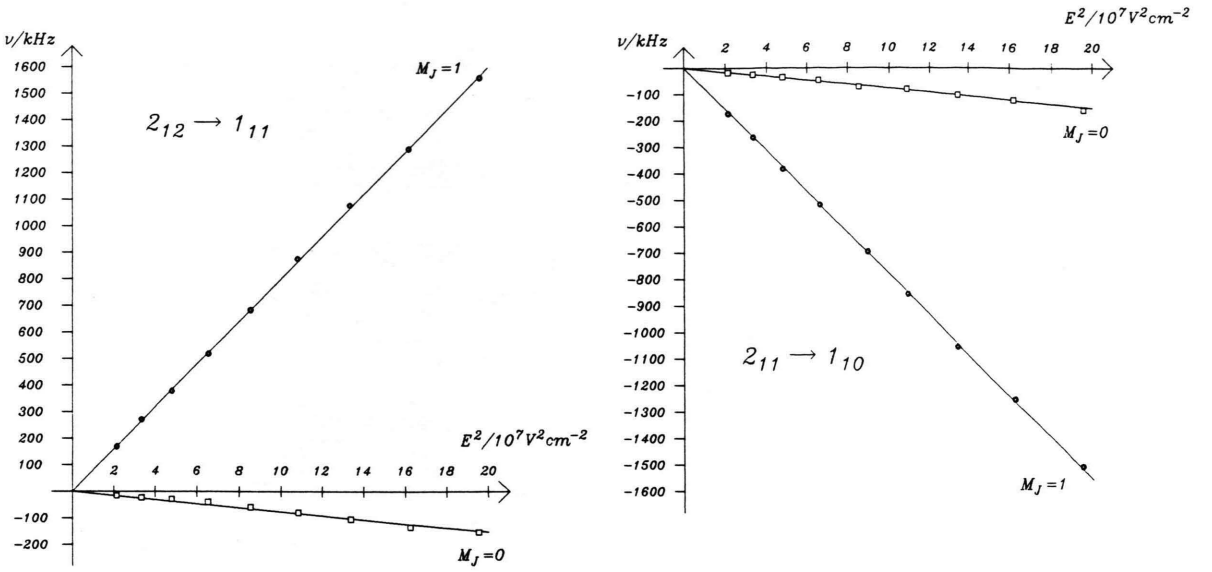

Fig. 3. Stark-splittings of the $2_{11} \rightarrow 1_{10}$ and $2_{12} \rightarrow 1_{11}$ rotational transitions plotted against the squared electric field strengths. For calibration of the field the Stark-effect of OCS was used, whose dipole moment and polarizability anisotropy are known with high precision.

latter are easily calculated from the closed analytical expressions for the rigid rotor energy levels as functions of the rotational constants [14] as derivatives with respect to the latter ([13], p. 125). Neglecting the small difference between α_{bb} and α_{cc} (see above), i.e. setting $\alpha_{bb}=\alpha_\perp=\alpha_{cc}$ and writing $\alpha_\parallel$ for α_{aa}, (5) can be rearranged into

$$W_{\alpha(J,K_aK_c,M)} = -\tfrac{1}{2}\alpha E_Z^2 + [a_{(J,K_aK_c)} + b_{(J,K_aK_c)} M^2]\, E_Z^2(\alpha_\parallel - \alpha_\perp) \quad (6)$$

with

$$a_{(J,K_aK_c)} = -\frac{J(J+1) - 3\langle \hat{J}_a^2\rangle}{3(2J-1)(2J+3)} \quad (7)$$

and

$$b_{(J,K_aK_c)} = \frac{J(J+1) - 3\langle \hat{J}_a^2\rangle}{(2J-1)(2J+3)\,J(J+1)}. \quad (8)$$

We now turn to the Stark-effect contribution which arises from the nonzero vibronic expectation value for the a-component of the electric dipole moment. Here second order perturbation theory leads to an energy expression with a form very similar to (6) [15]:

$$W_{\mu(J,K_aK_c\,M)} = [A_{(J,K_aK_c)} + B_{(J,K_aK_c)} M^2]\, E_Z^2\, \mu_a^2, \quad (9)$$

where the coefficients $A_{(J,K_aK_c)}$ and $B_{(J,K_aK_c)}$ are calculated as perturbation sums. Botskor's program KONABI was used for these calculations.

From (6) and (9) it follows that the Stark-shifts, if plotted against E_Z^2, should follow straight lines. This indeed is the case (compare Figure 3). We note that each observed Stark-shift corresponds to an equation which is linear in μ_a^2 and in the polarizability anisotropy, $(\alpha_\parallel - \alpha_\perp)$, with coefficients which can be calculated with high precision from the rotational constants. Thus the normal equations which correspond to the observed Stark-shifts listed in Table 1 were set up and were solved for μ_a^2 and $(\alpha_\parallel - \alpha_\perp)$. The fit leads to $|\mu_a| = 0.0053(2)$ D and $(\alpha_\parallel - \alpha_\perp) = 4.26(6) \cdot 10^{-24}$ cm^3 with a correlation coefficient between μ_a^2 and $(\alpha_\parallel - \alpha_\perp)$ equal to -0.010. The standard deviation of the fit is 6 kHz. (The numbers in brackets represent single standard deviations in units of the least significant digit.) With μ_a^2 and $(\alpha_\parallel - \alpha_\perp)$ known, also their individual contributions to the Stark-shifts can be calculated. They too are given in Table 1.

4. Discussion

The vibronic ground state expectation value for the electric dipole moment determined here, $\langle \mu_a \rangle = 0.0053(2)$ D, must be compared to the value determined from the broadening of the unresolved K_a-doublet $4_{32} \leftarrow 3_{31}$; $4_{31} \leftarrow 3_{30}$ upon application of a Stark-field [4]. A conventional 100 kHz Stark-modulation spectrometer had been used by the authors in their

pioneering study. In hindsight it is now obvious that the experimental uncertainty in the lineshape analysis (compare Fig. 2 in [4]) had been considerably underestimated and that the value for the electric dipole moment of $D_2C=C=CH_2$ has to be revised. As a consequence, all studies which have used this older value for $\langle\mu_a\rangle$, for instance for calibration purposes, have to be reexamined too. As an example we quote the vibronic expectation values of $H_2C=C=CH_2$ in its degenerate vibrational states $v_{10}=1$ and $v_{11}=1$. These values have been determined in an elegant MWFT double resonance experiment by Vogelsanger and Bauder (compare Table III in [8]). Unfortunately no experimental values were given by the authors but roughly, i.e. neglecting that also a slightly changed value for the polarizability anisotropy should be used, their reported values will have to be upscaled by the quotient of the two dipole expectation values, i.e. by 53/31 (compare (2) in [8]).

We now turn to our result for the static polarizability anisotropy. We believe that its fairly accurate value should be of interest for scaling the results of semiempirical and ab initio quantum chemical calculations. (Recently quantum chemical calculations of the static polarizabilities and hyperpolarizabilities of polyenes have been reported in increasing numbers in an attempt to assist experimental chemists in their search for new products with interesting technical properties, cf. [16–19].) For such comparisons we complement the value for the anisotropy as determined in this work by a value for the static bulk polarizability as it may be extrapolated from the optical gas phase polarizabilities $(a_{\parallel}-a_{\perp})$ determined by Buckingham and coworkers [20]. We extrapolated their optical (or electronic) contributions to the polarizabilities to zero frequency under the assumption that they are linear functions in ν^2 (ν = optical frequency) (cf. [21], p. 3323 lower right). The static molecular bulk polarizability was then estimated using the crude relation [22]

$$\alpha=\frac{(\alpha_{\parallel}-\alpha_{\perp})}{(a_{\parallel 0}-a_{\perp 0})}\cdot a_0\,. \tag{10}$$

In (10) $a_0=5.99\cdot 10^{-24}\,\mathrm{cm}^3$ and $(a_{\parallel 0}-a_{\perp 0})=4.55\cdot 10^{-24}\,\mathrm{cm}^3$ are the electronic contributions to the static bulk polarizability and static polarizability anisotropy, respectively, as extrapolated by the procedure outlined above. From (10) we obtain $\alpha=(\alpha_{\parallel}-2\alpha_{\perp})/3=5.61\cdot 10^{-24}\,\mathrm{cm}^3$. Combined with our experimental value for the susceptibility anisotropy this leads to the individual components for the static polarizability tensor of allene: $\alpha_{\parallel}=8.4_5\cdot 10^{-24}\,\mathrm{cm}^3$ and $\alpha_{\perp}=4.1_9\cdot 10^{-24}\,\mathrm{cm}^3$. In view of the unknown error introduced by the use of (10) we do not quote uncertainties for these values. We believe, however, that their uncertainties should correspond to single standard deviations of approximately $\pm 0.1\cdot 10^{-24}\,\mathrm{cm}^3$. Finally we compare the experimental results to the corresponding values computed by the Hartree Fock SCF-routine from the Gaussian 88 program package [23] installed at the VAX-X-MC at the computer center at the University of Kiel (see Table 2). The 6-311 G** basis was used and the calculation was carried out at the experimental r_0-structure, as fitted to the rotational constants of $HDC=C=CH_2$ and $D_2C=C=CH_2$ ($r_{(C=C)}=1.3095(8)$ Å, $r_{(C-H)}=1.0835(24)$ Å, and $<HCH=118.55(25)°$). With the computed value for $(\alpha_{\parallel}-\alpha_{\perp})$ at about 150% of the experimental value, the necessity for calibration of quantum chemical results is obvious. This will be especially true for lower level quantum chemical calculations such as have to be used presently for approximate calculations of the properties of larger polyenes.

Table 2. Comparison of the experimental values for the static polarizabilities of allene, $H_2C=C=CH_2$, with Hartree-Fock values calculated for the microwave r_0-structure $r_{C=C}=1.3095(8)$ Å, $r_{C-H}=1.0835(24)$ Å, $<HCH=118.55(25)°$ (compare [15] for the different structure definitions).

Method	$(\alpha_{\parallel}-\alpha_{\perp})/\text{Å}^3$	$\alpha/\text{Å}^3$	$\alpha_{\parallel}/\text{Å}^3$	$\alpha_{\perp}/\text{Å}^3$
HF-SCF (6-311 G**)	6.06	4.98	9.02	2.96
Exp. this work and [20]	4.26(6)	5.61	8.45	4.19

Acknowledgements

We would like to thank Prof. H. Dreizler for providing the V-band parts and many helpful discussions, the members of the machine shop of the institute for their elaborate and precise manufacturing of the Stark-cells, and Prof. A. Guarnieri for critically reading the manuscript. The work was funded by Deutsche Forschungsgemeinschaft under Grant Su 42/14-2.

[1] J. C. McGurk, T. G. Schmalz, and W. H. Flygare, Adv. Chem. Phys. **25,** 1 (1974).
[2] E. Fleige and H. Dreizler, Z. Naturforsch. **42a,** 72 (1987).
[3] O. Böttcher, N. Heineking, and D. H. Sutter, J. Mol. Spectrosc. **139,** 236 (1990).
[4] E. Hirota and C. Matsumura, J. Chem. Phys. **59,** 3038 (1973).
[5] Ch. Keussen, N. Heineking, and H. Dreizler, Z. Naturforsch. **44a,** 215 (1989).
[6] U. Andresen and B. Kleibömer, Rev. Sci. Instrum. **59,** 1088 (1988).
[7] B. Kleibömer and D. H. Sutter, Z. Naturforsch. **43a,** 561 (1988).
[8] B. Vogelsanger and A. Bauder, J. Chem. Phys. **87,** 4465 (1987).
[9] K. Tanaka, H. Ito, K. Harada, and T. Tanaka, J. Chem. Phys. **80,** 5893 (1984).
[10] O. Böttcher and D. H. Sutter, Z. Naturforsch. **43a,** 47 (1988).
[11] J. Haekel and H. Mäder, Z. Naturforsch. **43a,** 203 (1988).
[12] S. Golden and E. Bright Wilson Jr., J. Chem. Phys. **16,** 669 (1948).
[13] D. H. Sutter and W. H. Flygare, Top. Curr. Chem. **63,** 89 (1976).
[14] cf. G. M. Barrow, Introduction to Molecular Spectroscopy, McGraw-Hill Kogakusha Ltd., Int. Student Ed. (1962), Table 5-4.
[15] W. Gordy and R. L. Cook, Microwave Molecular Spectra, John Wiley & Sons, New York 1984, Chapter X,3.
[16] J. A. Yoffe, Theor. Chim. Acta **51,** 107 (1979).
[17] N. G. Papadopoulos, J. Waite, and C. A. Nicolaides, J. Chem. Phys. **77,** 2527 (1982).
[18] J. Delhalle, V. P. Bodart, M. Dory, J. M. Andre, and J. Zyss, Int. J. Quantum Chem.; Quant. Chem. Symp. **19,** 313 (1986).
[19] A. K. Chandra and M. Banerjee, J. Molec. Struct. (Theochem) **236,** 193 (1991).
[20] M. P. Bogaard, A. D. Buckingham, R. K. Pierens, and A. H. White, J. Chem. Soc. Faraday Transact. **74,** 3008 (1978).
[21] G. R. Alms, A. K. Burnham, and W. H. Flygare, J. Chem. Phys. **63,** 3321 (1975).
[22] A. D. Buckingham, M. P. Bogaard, D. A. Dunmur, C. P. Hobbs, and B. J. Orr, Trans. Farad. Soc. **66,** 1548 (1970).
[23] M. J. Frisch, J. S. Binkley, H. B. Schlegel, K. Raghavachari, C. F. Melius, R. L. Martin, J. J. P. Steart, F. W. Bobrowicz, C. M. Rohlfing, L. P. Kahn, D. J. Defrees, R. Seeger, R. A. Whiteside, D. C. Fox, E. M. Fluder, and J. A. Pople, Gaussian Inc., Pittsburgh, USA.